Electronic structure and optical responses of nanocrystalline BiGaO3 films: A combination study of experiment and theory

J. Z. Zhang, H. C. Ding, J. J. Zhu, Y. W. Li, Z. G. Hu, C. G. Duan, X. J. Meng, and J. H. Chu

Citation: Journal of Applied Physics **115**, 083110 (2014); doi: 10.1063/1.4867006
View online: http://dx.doi.org/10.1063/1.4867006
View Table of Contents: http://scitation.aip.org/content/aip/journal/jap/115/8?ver=pdfcov
Published by the AIP Publishing

Electronic structure and optical responses of nanocrystalline $BiGaO_3$ films: A combination study of experiment and theory

J. Z. Zhang (张金中),[1,2] H. C. Ding (丁航晨),[1] J. J. Zhu (诸佳俊),[1,2] Y. W. Li (李亚巍),[1] Z. G. Hu (胡志高),[1,a)] C. G. Duan (段纯刚),[1,2] X. J. Meng (孟祥建),[2] and J. H. Chu (褚君浩)[1,2]

[1]*Key Laboratory of Polar Materials and Devices, Ministry of Education, Department of Electronic Engineering, East China Normal University, Shanghai 200241, China*

[2]*National Laboratory for Infrared Physics, Shanghai Institute of Technical Physics, Chinese Academy of Science, Shanghai 200083, China*

(Received 21 January 2014; accepted 14 February 2014; published online 27 February 2014)

High-quality nanocrystalline $BiGaO_3$ (BGO) films have been prepared by a modified sol-gel method. X-ray diffraction analysis shows that the films are polycrystalline and exhibit an orthorhombic structure. The dispersion functions near infrared-ultraviolet region were extracted by fitting spectroscopic ellipsometry with the Tauc-Lorentz model. Moreover, first-principle calculations on dielectric functions and band gap were carried out, which are in good agreement with the experimental results. It was found that BGO belongs to an indirect band gap oxide with the fundamental gap of about 2.17 eV, which is suitable for ferroelectric based photovoltaic devices. © *2014 AIP Publishing LLC*. [http://dx.doi.org/10.1063/1.4867006]

I. INTRODUCTION

Bi-containing perovskites and perovskite-related materials such as $BiAlO_3$, $BiGaO_3$ (BGO), $BiInO_3$, $Bi_4Ti_3O_{12}$, $BiFeO_3$, and $BiMnO_3$ have received a lot of attention as lead-free ferroelectrics, ferromagnetic, and photovoltaic materials.[1–5] As promising oxides, $BiAlO_3$ and $BiGaO_3$ are predicted that they should be high performance piezoelectrics and ferroelectrics with large spontaneous polarization from the hypothetical perovskite structure.[6] Experimentally, bulk perovskite-like $BiAlO_3$ and pyroxene-like $BiGaO_3$ have been synthesized using a high-pressure and high-temperature technique and their structure parameters were refined.[7] Recently, $BiAlO_3$ thin films on $SrRuO_3$/(100)$LaAlO_3$ substrates with a pseudotetragonal symmetry have been deposited by pulsed laser deposition. It was reported that the $BiAlO_3$ film showed a good ferroelectric property with a remanent polarization of about 29 $\mu C/cm^2$.[8] Unfortunately, the synthesis and physicochemical properties of $BiGaO_3$ films have not been reported.

In the last decade, pure and element-doped bulk BGO have been investigated by theoretical and experimental methods. Theoretically, Baettig *et al*. predicted that BGO has a polarization of about 152 $\mu C/cm^2$ along the [100] direction and a e_{33} piezoelectric constant of about -165.4 ± 1.2 $\mu C/cm^2$ (change in polarization along [100] when the strain is applied along [100]).[6] Wang *et al*. performed the density functional theory (DFT) with the generalized gradient approximation to investigate the crystal structure, electronic properties, zone-center phonon modes, dielectric properties, structural instability, and its driving force of BGO. It was found that it is a semiconductor with an indirect band gap of about 1.34 eV ($M \rightarrow X$ point).[9] Moreover, Li *et al*. have confirmed that BGO belongs to the orthorhombic structure (Space group *Pcca*) rather than the cubic phase and presents a direct band gap of about 2.03 eV at *X* point.[10] It should be emphasized that the band gap is smaller than that (2.6 eV) of $BiFeO_3$, which can generate large photovoltages up to 15 V.[2] Experimentally, pyroxene-like BGO was synthesized using a high-pressure and high-temperature technique at 6 GPa and 1473 K. Its crystal structure was refined by neutron powder diffraction data in centrosymmetric space group *Pcca*.[7] Its high-pressure phase transitions were investigated by analyzing Raman active models, such as A_g, B_{1g}, B_{2g}, and B_{3g}.[11] Moreover, solid solutions of $BiGa_xM_{1-x}O_3$ (M = Cr, Mn, and Fe) were also prepared using a high pressure and temperature method and their structural phase transitions were characterized by X-ray powder diffraction.[3] Recently, it is reported that the $BiFe_{0.9}Ga_{0.1}O_3$ films on $LaNiO_3$/glass substrates prepared by a chemical-solution deposition exhibit a huge ferroelectric polarization of 230 $\mu C/cm^2$ at room temperature since the coexistence of *R*3*c* and *Cm* phases, which induces the lattice instability and changes the switching paths of polarization.[12] However, few reports on optical properties of pure and element-substituted $BiGaO_3$ films have been presented, which is an important aspect as a potential photovoltaic material.

In this work, we report that BGO films with an orthorhombic structure can be simply prepared using a modified sol-gel method at air pressure. Its dielectric functions have been extracted by fitting the measured ellipsometric spectra with a five phase layered (air/surface rough layer (SRL)/BGO/LNO/Si) model and the Tauc-Lorentz (TL) dispersion model in the photon energy range of 0.5-4.0 eV. The Tauc behavior analysis of BGO films indicates that it is an indirect band gap semiconductor ($E_{g,Tauc}^{ind} \sim 2.17$ eV), which is in good agreement with the theoretical predictions.

II. EXPERIMENTAL DETAILS

The BGO films on (100)LNO/Si substrates were fabricated by a modified sol-gel method. Analytically pure

a)Author to whom correspondence should be addressed. Electronic mail: zghu@ee.ecnu.edu.cn. Tel.: +86-21-54345150. Fax: +86-21-54345119.

bismuth nitrate [$Bi(NO_3)_3 \cdot 5H_2O$, 99.0%] and Gallium(III) nitrate hydrate [$Ga(NO_3)_3 \cdot 6H_2O$, 99.9%] were dissolved in heated glacial acetic acid (CH_3COOH, 99.5%) with magnetic stirring until the 0.1 M (Bi and Ga)-precursor solution was stable and homogeneous. Note that an appropriate amount of acetylacetone ($C_5H_8O_2$, 99.0%) was added into the solution as a chelating agent and excess 6 mol% Bi source was added for compensating the Bi evaporation during the annealing process. The precursor solutions were stabilized for about 30 days to enhance the hydrolysis and polymerization. Before the deposition of the BGO films, pseudocubic (100) LNO films on silicon substrates were prepared by magnetron radio frequency (13.6 MHz) sputtering at the argon gas pressure of 2 Pa and *in situ* annealed at 265 °C. The experimental details can be found elsewhere.[13] Then, the BGO films were deposited by spin coating the (Bi and Ga)-precursor solution onto the (100)LNO substrates at a speed of 4000 rpm for 20 s. Each layer of the films was dried in ambient air by a rapid thermal annealing procedure. The deposition and annealing-treatment procedures were repeated eight times to obtain the desired thickness. The crystalline structure of BGO films was investigated by X-ray diffraction (XRD) using a Ni filtered Cu Kα radiation source (D/MAX-2550 V, Rigaku Co.). The surface morphology of the films was examined by atomic force microscopy (AFM; Digital Instruments Dimension Icon, Bruker). The scale height and measured area are 30 nm and $5 \times 5\ \mu m^2$, respectively. The thickness was examined by field emission scanning electron microscopy (FESEM; Philips XL30FEG). The ellipsometric measurements were carried out by a near-infrared-ultraviolet (NIR-UV) spectroscopic ellipsometry (SE) in the wavelength range of 310-2500 nm (0.5–4.0 eV) with a spectral resolution of 2 nm (V-VASE by J. A. Woollam Co., Inc.). Computations were performed at the ECNU computing center.

III. RESULTS AND DISCUSSION

Figure 1 illustrates that the LNO films are pseudocubic perovskite crystal structure with the (100) preferred orientation and the lattice constant a (b or c) is about 3.87 Å, which is slightly larger than that of powder material (3.84 Å) according to the JCPDS card (No. 33-0710). The inset of Figure 1 shows the orthorhombic crystal structure of BGO and its unit cell includes four formulas ($Bi_4Ga_4O_{12}$). In the case of BGO films, there are (112), (011), (224) and some other weaker diffraction peaks, which confirms that the film is polycrystalline and has the orthorhombic structure. Based on the (112), (011), and (224) diffraction peaks, the lattice constants a, b, and c can be estimated to be 5.626, 5.081, and 10.339 Å, respectively. Moreover, the average grain size of the BGO film is estimated to be about 22 nm from the (112) diffraction peak according to the well-known Scherrer equation.[14] The three-dimensional AFM images of BGO films suggest that the surface morphology is smooth with the root-mean-square roughness of about 4.5 nm [Figure 2(a)]. The cross-section SEM of the BGO/LNO films on Si substrates shows that the interface of the BGO and LNO films is distinct because the two films have different textures as shown in Figure 2(b). The thicknesses of BGO and LNO

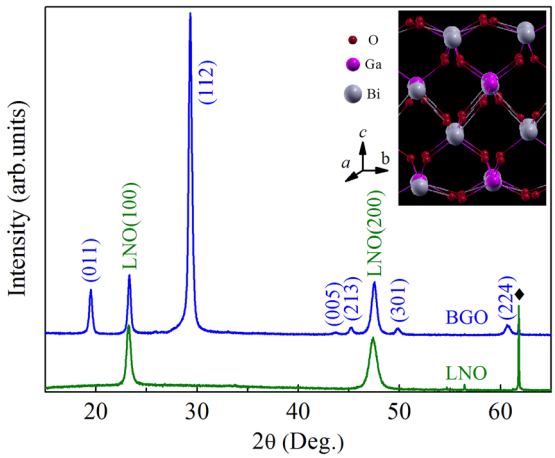

FIG. 1. X-ray diffraction patterns of the (100)LNO and BGO/(100)LNO films on Si substrates. The inset shows the orthorhombic crystal structure of $BiGaO_3$. The Bi, Ga, and O atoms are denoted by the spheres with different sizes and colors. Not that the symbol "◆" indicates the diffraction peak of Si substrates.

films were estimated to be about 102 ± 10 and 112 ± 10 nm, respectively.

The experimental $\Psi(E)$ and $\Delta(E)$ spectra recorded at room temperature for the BGO films on LNO/Si substrates are shown by the dotted lines in Figures 2(c) and 2(d), respectively. The incident angle was selected to 70° for the BGO/LNO films corresponding to the experimental optimization near the Brewster angle of silicon. In order to extract optical band gap, dielectric functions, and other physical parameters of BGO films, the ellipsometric spectra measured at room temperature were fitted by a five-layer structure (air/surface rough layer/BGO/LNO/Si). Specifically, the Brüggeman effective medium approximation was employed to calculate the effective dielectric functions $\tilde{\varepsilon}_{eff}(E)$ of the SRL, which is described by the assumption 50% void component $\tilde{\varepsilon}_v(E)$ and 50% BGO film component $\tilde{\varepsilon}_f(E)$ in the present case (i.e., $0 = 50\% \cdot \frac{\tilde{\varepsilon}_v(E)-\tilde{\varepsilon}_{eff}(E)}{\tilde{\varepsilon}_v(E)-2\tilde{\varepsilon}_{eff}(E)} + 50\% \cdot \frac{\tilde{\varepsilon}_f(E)-\tilde{\varepsilon}_{eff}(E)}{\tilde{\varepsilon}_f(E)-2\tilde{\varepsilon}_{eff}(E)}$).[15,16] Moreover, the TL model is an effective

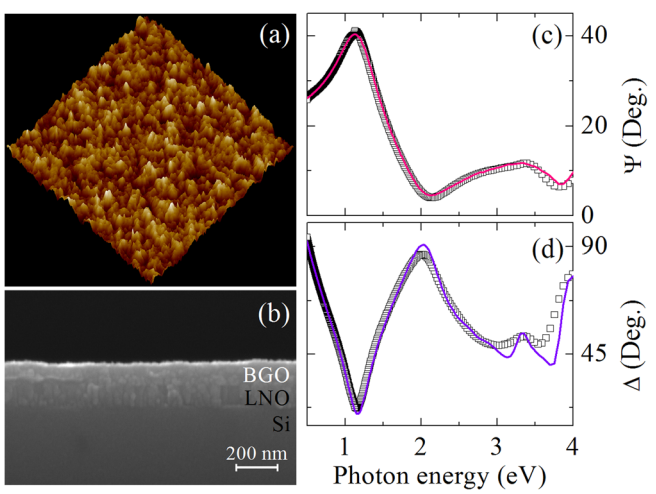

FIG. 2. (a) Three-dimensional atomic force microscopy images and (b) cross-sectional scanning electron microscopy images of BGO/LNO films on Si substrates. The near infrared-ultraviolet experimental (dotted lines) and best-fitted (solid lines) ellipsometric spectra (c) Ψ and (d) Δ of BGO/LNO films.

model to express the dielectric functions of the BGO films at the photon energies below and above fundamental band gap.[17,18] Accurately, the imaginary part of the dielectric functions $\varepsilon_i(E)$ in the TL model can be written as: $\varepsilon_i(E) = A_0E_nC(E-E_g)^2/[E(E^2-E_n^2)^2+C^2E^3], \quad (E \geq E_g)$ and $\varepsilon_i(E) = 0, (E < E_g)$, where A_0, E_n, C, and E_g are the transition matrix element, peak transition energy, broadening term, and Tauc gap energy, respectively. Correspondingly, the real part $\varepsilon_r(E)$ can be derived by the Kramers-Krönig transformation: $\varepsilon_r(E) = 1 + 2\pi^{-1}P\int_{E_g}^{\infty} \xi\varepsilon_i(\xi)/(\xi^2-E^2)d\xi$. As a kind of metal oxide, the dielectric functions of LNO films can be characterized very well by the Drude-Lorentz dispersion model, which can be written as:[19,20] $\tilde{\varepsilon}(E) = \varepsilon_\infty - A_D/(E^2+iEB_D) + \Sigma_{j=1}^{3}A_j/(E_j^2-E^2-i\Gamma_jE)$. Here, ε_∞ is the high-frequency dielectric constant, A_D is the square of plasma frequency, and B_D is the electron collision or damping frequency. A_j, Γ_j, E_j, and E are the amplitude, broadening center, energy of the jth oscillator, and incident photon energy, respectively. Finally, the optical constants of the Si substrate in the fitting process can be directly taken from Ref. 21. The Levenberg-Marquardt algorithm was used in the linear least-squares curve fitting. A root mean-square fractional error function has been used to judge the fitting quality between the experimental and modeled data.[22] The best-fitted ellipsometric spectra $\Psi(E)$ and $\Delta(E)$ of BGO/LNO films on silicon substrates are shown by the solid lines in Figures 2(c) and 2(d), respectively. The fitted values of the thicknesses for SRL (2.8 ± 0.4 nm), BGO (91.7 ± 0.9 nm), and LNO (101.5 ± 0.9 nm) films are consistent with those derived from the AFM and SEM pictures. The best-fit parameter values in the dispersion functions of the BGO/LNO films were listed in Table I. It should be pointed out that the Tauc gap energy of BGO films is about 2.64 ± 0.01 eV.

Ab initio DFT calculations based on the projector augmented wave method (PAW) are conducted by using the Vienna *ab initio* Simulation Package (VASP).[23,24] Local density approximation (LDA) for exchange and correlation is employed along with a standard plane-wave basis set with a kinetic-energy cutoff of 500 eV. These calculations are performed by using the $8 \times 8 \times 4$ Monkhorst-Pack k-point mesh,[25] and the convergence criterion for the electronic energy is 10^{-5} eV. The orthorhombic crystal structure with the space group *Pcca* (inset of Figure 1) is adopted. Comparing with experimental values, the calculated lattice constants ($a = 5.369$, $b = 5.148$, and $c = 9.745$ Å) are underestimated, but it is not atypical consequence of the LDA. The results of optical calculation are based on the independent-particle approximation using our own code OPTICPACK.[26] We can write the interband optical conductivity tensor as: $\sigma(\omega) = 2\pi/\omega\Omega\sum_{\mathbf{k}} W_{\mathbf{k}} \sum_{c,v} |\langle c|\boldsymbol{e}\cdot\boldsymbol{p}|v\rangle|^2\delta(E_c - E_v - \omega)$, where Ω is the cell volume, ω is the photon energy, $\boldsymbol{e}$ is the polarization direction of the photon, and $\boldsymbol{p}$ is the electron momentum operator. The integral over the $\boldsymbol{k}$-space has been replaced by a summation over special k-points with corresponding weighting factors $W_{\mathbf{k}}$. The second summation includes the valence-band states (v) and conduction-band states (c), and E is the corresponding band energy. The imaginary part of the complex dielectric function (ε_i) is then evaluated from the optical conductivity. The real part of the dielectric function (ε_r) is obtained by the Kramers-Krönig relation.

TABLE I. The dielectric function parameters for the BGO and LNO films determined from the simulation of ellipsometric spectra in Figure 1. The 90% reliability of the fitting parameters is given in parentheses.

BGO					
$\varepsilon_{\infty 1}$	A_0 (eV)	E_g (eV)	E_n (eV)	C (eV)	–
4.09	69	2.64	3.89	1.47	–
(0.02)	(2)	(0.01)	(0.02)	(0.05)	–
LNO					
$\varepsilon_{\infty 2}$	A_D (eV)	B_D (eV)	A_1 (eV^2)	Γ_1 (eV)	E_1 (eV)
2.59	5.41	1.37	1.43	1.23	1.19
(0.11)	(0.02)	(0.08)	(0.11)	(0.05)	(0.01)
A_2 (eV^2)	Γ_2 (eV)	E_2 (eV)	A_3 (eV^2)	Γ_3 (eV)	E_3 (eV)
0.27	0.95	2.22	0.76	1.92	3.08
(0.07)	(0.12)	(0.02)	(0.08)	(0.27)	(0.05)

The band structure and density of states (DOS) of orthorhombic BGO are shown in Figure 3. Specifically, the energy bands at around -10 eV derived from the Bi 6s states. The energy bands between -8 and -6 eV are mainly composed of Ga 4s states. The BGO appears to have some covalent feature since O 2p states have some admixture with Bi 6p and Ga 4p states within the energy window from -6 to -2 eV. More importantly, the top of valence bands (VBs) and bottom of conduction bands (CBs) consist of O 2p and Bi 6p states, respectively, and the result is consistent with previous work.[10] It is found that BGO is an indirect band gap material of about 1.95 eV from the top of valence bands located between the Γ and Y points to the bottom of conduction bands located at the X point, while its direct transition happens at the X point of about 2.01 eV. It should be emphasized

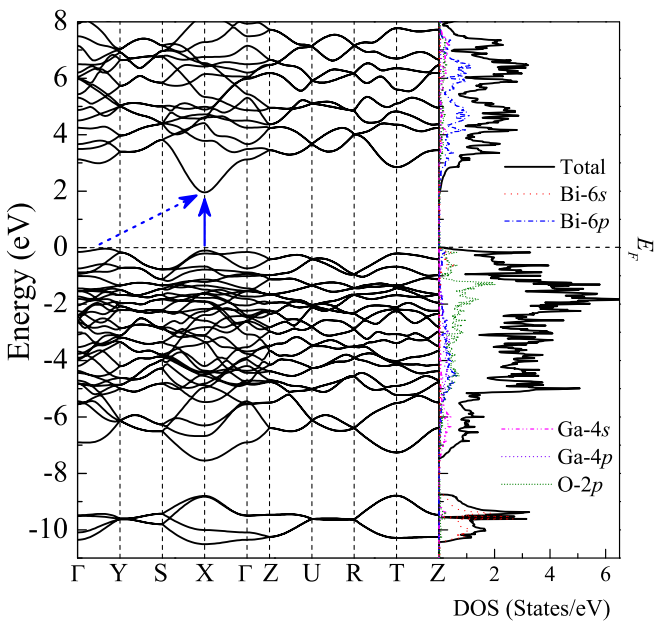

FIG. 3. Calculated band structure and DOS of orthorhombic $BiGaO_3$. The solid and dashed arrows indicate the direct and indirect electron transitions, respectively.

that the band gap predicted by DFT is less than the experimental value of about 2.64 eV derived from the TL model. It means that our experimental result overestimates its real band gap. Accurately, the real band gap is below the Tauc gap energy due to Urbach tails, which are not included in the TL dispersion model.

As a potential photovoltaic material, the optical conductivity of BGO films was illustrated in Figure 4(a). It suggests that the real part of optical conductivity values are similar to that of ferroelectric $Bi_4Ti_3O_{12}$, whose band gap is quite large (3–4 eV) for photovoltaic devices.[27] Based on the relationship between optical conductivity and dielectric functions, the real $\varepsilon_r(E)$ and imaginary $\varepsilon_i(E)$ parts of the dielectric functions (solid lines) in a wider photon energy range were calculated. The experimental dielectric functions (dotted lines) deduced by fitting the spectroscopic ellipsometry of BGO film are in agreement with the theoretical results, which are shown in Figure 4(b). Generally, BGO material is transparent in the lower photon energy region below 2 eV, where the value of $\varepsilon_i(E)$ is very small and even zero. The calculated static refractive index $n(0)$ $[\tilde{n}(E) = \sqrt{\tilde{\varepsilon}_r(E)}]$ is about 2.34. With increasing the photon energy, the ε_r increases and approaches the maximum of about 8.8 at around 3.5 eV, then decreases because of the well-known Van Hove singularities.[28] In the absorption region above the optical band gap, the peaks of the $\varepsilon_i(E)$ spectrum at around 4.37, 5.23, 6.68, and 7.93 eV correspond to the electron transitions from the O 2*p* states in VB to the Bi 6*p* ones in CB. Furthermore, the higher energy absorptions are mainly the electron transitions from O 2*p* to Ga 4*s* states. It should be emphasized that there exists a deviation between experimental and theoretical $\varepsilon_i(E)$ at the absorption edge because the TL model does not include Urbach tails $U(E, T)$, which is a function of temperature.[29] In addition, the indirect band gap of BGO is also estimated by using the traditional Tauc relation: $(\alpha E)^n = A(E - E_{g,Tauc})$, where α is absorption coefficient, A is the edge width parameter representing film quality, E is the photon energy, $E_{g,Tauc}$ is the optical band gap, and the exponent n is a characteristic of type in optical transition process ($n = 2$ for direct transition and $n = 1/2$ for indirect one).[30] For the case of indirected band gap BGO, experimental and theoretical $(\alpha E)^{1/2}$ versus photon energy E were plotted as shown in Figures 4(c) and 4(d), respectively. The value of the indirect band gap $E^{ind}_{g,Tauc}$ of about 2.17 eV was determined from the intercept of the extrapolation to zero absorption with the photon energy axis. By combining experimental and theoretical data, the Urbach bandtail energy (E_U) at room temperature is obtained of about 0.5 eV, which may originate from defects in the lattice and short-time localization of exciton mode coupling to lattice distortion.[29]

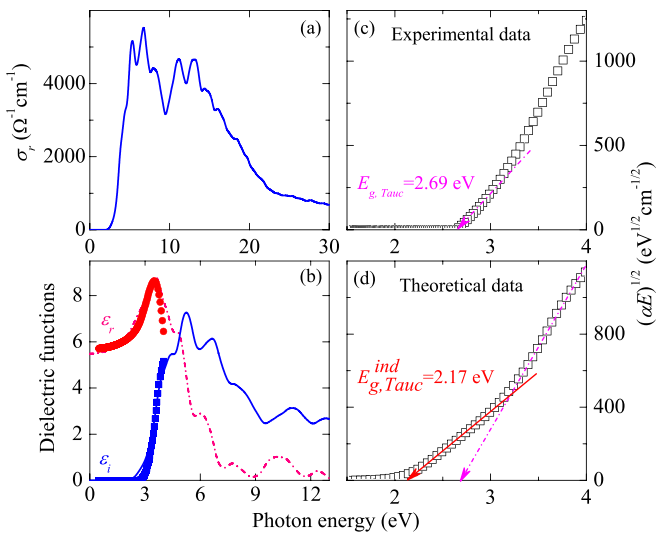

FIG. 4. (a) Real part σ_r of optical conductivity for $BiGaO_3$ as a function of photon energy. (b) Experimental evolution (dotted lines) and theoretical prediction (solid lines) real part $\varepsilon_r(E)$ and imagine part $\varepsilon_i(E)$ of dielectric functions. (c) Experimental and (d) theoretical $E_{g,Tauc}$ and $E^{ind}_{g,Tauc}$ determination based on the Tauc's law. The solid and dashed arrows indicate the $E^{ind}_{g,Tauc}$ and $E_{g,Tauc}$ band gap, respectively.

IV. CONCLUSIONS

In summary, high quality BGO films on LNO/Si substrates have been prepared by a modified sol-gel method. X-ray diffraction analysis shows that the films are polycrystalline and exhibit orthorhombic structure with the lattice constants $a = 5.626$, $b = 5.081$, and $c = 10.339$ Å. The dielectric functions in the NIR-UV region for BGO films were extracted by fitting spectroscopic ellipsometry with the Tauc-Lorentz model. Finally, it was found that the BGO films can be used in photovoltaic devices since its band gap is about 2.17 eV. The Urbach bandtail energy (E_U) at room temperature is about 0.5 eV, which originates from defects in the lattice and short-time localization of exciton mode coupling to lattice distortion.

ACKNOWLEDGMENTS

One of the authors (J. Z. Zhang) would like to thank Dr. Yude Shen, Liping Xu, and Pengpeng Jiang for technical supports. This work was financially supported by Major State Basic Research Development Program of China (Grant Nos. 2011CB922200 and 2013CB922300), Natural Science Foundation of China (Grant Nos. 11374097, 61376129, 61106122, and 61125403), Projects of Science and Technology Commission of Shanghai Municipality (Grant Nos. 13JC1402100 and 13JC1404200), the Program for Professor of Special Appointment (Eastern Scholar) at Shanghai Institutions of Higher Learning.

[1]I. Grinberg, D. V. West, M. Torres, G. Gou, D. M. Stein, L. Wu, G. Chen, E. M. Gallo, A. R. Akbashev, P. K. Davies, J. E. Spanier, and A. M. Rappe, Nature **503**, 509 (2013).
[2]S. Y. Yang, J. Seidel, S. J. Byrnes, P. Shafer, C. H. Yang, M. D. Rossell, P. Yu, Y. H. Chu, J. F. Scott, J. W. Ager III, L. W. Martin, and R. Ramesh, Nat. Nanotechnol. **5**, 143 (2010).
[3]A. A. Belik, D. A. Rusakov, T. Furubayashi, and E. Takayama-Muromachi, Chem. Mater. **24**, 3056 (2012).
[4]A. Singh, C. Moriyoshi, Y. Kuroiwa, and D. Pandey, Phys. Rev. B **88**, 024113 (2013).
[5]R. de Sousa, M. Allen, and M. Cazayous, Phys. Rev. Lett. **110**, 267202 (2013).
[6]P. Baettig, C. F. Schelle, R. LeSar, U. V. Waghmare, and N. A. Spaldin, Chem. Mater. **17**, 1376 (2005).
[7]A. A. Belik, T. Wuernisha, T. Kamiyama, K. Mori, M. Maie, T. Nagai, Y. Matsui, and E. Takayama-Muromachi, Chem. Mater. **18**, 133 (2006).

[8]J. Y. Son, C. S. Park, and Y.-H. Shin, Appl. Phys. Lett. **92**, 222911 (2008).
[9]H. Wang, B. Wang, Q. Li, Z. Zhu, R. Wang, and C. H. Woo, Phys. Rev. B **75**, 245209 (2007).
[10]C. L. Li, B. Wang, R. Wang, H. Wang, and X. Y. Lu, Comput. Mater. Sci. **42**, 614 (2008).
[11]H. Yusa, A. A. Belik, E. Takayama-Muromachi, N. Hirao, and Y. Ohishi, Phys. Rev. B **80**, 214103 (2009).
[12]J. Yan, M. Gomi, T. Yokota, and H. Song, Appl. Phys. Lett. **102**, 222906 (2013).
[13]Q. Zhao, Z. M. Huang, Z. G. Hu, and J. H. Chu, Surf. Coat. Technol. **192**, 336 (2005).
[14]A. L. Patterson, Phys. Rev. **56**, 978 (1939).
[15]D. A. G. Brüggeman, Ann. Phys. (Berlin) **416**, 636 (1935).
[16]H. Fujiwara, J. Koh, P. I. Rovira, and R. W. Collins, Phys. Rev. B **61**, 10832 (2000).
[17]G. E. Jellison, Jr. and F. A. Modine, Appl. Phys. Lett. **69**, 371 (1996); **69**, 2137 (1996).
[18]X. Chen, K. Jiang, Z. G. Hu, X. F. Chen, G. S. Wang, X. L. Dong, and J. H. Chu, Appl. Phys. Lett. **101**, 011914 (2012).
[19]B. Berini, N. Keller, Y. Dumont, E. Popova, W. Noun, M. Guyot, J. Vigneron, A. Etcheberry, N. Franco, and R. M. C. da Silva, Phys. Rev. B **76**, 205417 (2007).
[20]J. J. Zhu, W. W. Li, Y. W. Li, Y. D. Shen, Z. G. Hu, and J. H. Chu, Appl. Phys. Lett. **97**, 211904 (2010).
[21]C. M. Herzinger, B. Johs, W. A. McGahan, J. A. Woollam, and W. Paulson, J. Appl. Phys. **83**, 3323 (1998).
[22]J. A. Woollam, *Guide to Using WVASE 32: Software for Spectroscopic Ellipsometry Data Acquisition and Analysis* (J A Woollam Co., Inc., 2005).
[23]P. E. Blöchl, Phys. Rev. B **50**, 17953 (1994).
[24]G. Kresse and J. Furthmuller, Comput. Mater. Sci. **6**, 15 (1996).
[25]H. J. Monkhorst and J. D. Pack, Phys. Rev. B **13**, 5188 (1976).
[26]G. Y. Guo, K. C. Chu, D.-S. Wang, and C.-G. Duan, Phys. Rev. B **69**, 205416 (2004).
[27]D. J. Singh, S. S. A. Seo, and H. N. Lee, Phys. Rev. B **82**, 180103 (2010).
[28]L. Van Hove, Phys. Rev. **89**, 1189 (1953).
[29]M. Letz, A. Gottwald, M. Richter, and L. Parthier, Phys. Rev. B **79**, 195112 (2009).
[30]G. He, L. D. Zhang, G. H. Li, M. Liu, and X. J. Wang, J. Phys. D: Appl. Phys. **41**, 045304 (2008).